Nonlinear Control of Electromagnetic Topological Edge States

D. A. Dobrykh, A. V. Yulin, A. P. Slobozhanyuk, A. N. Poddubny, and Yu. S. Kivshar

Nonlinear control of electromagnetic topological edge states

D. A. Dobrykh[1], A. V. Yulin[1], A. P. Slobozhanyuk[1,2], A. N. Poddubny[2,1,3], Yu. S. Kivshar[1,2]

[1]*ITMO University, St. Petersburg 197101, Russia*
[2]*Nonlinear Physics Center, Australian National University, Canberra ACT 2601, Australia*
[3]*Ioffe Physical-Technical Institute of the Russian Academy of Sciences, St. Petersburg 194021, Russia*

Topological photonics has emerged recently as a smart approach for realizing robust optical circuitry, and the study of nonlinear effects is expected to open the door for tunability of photonic topological states. Here we realize experimentally nonlinearity-induced spectral tuning of electromagnetic topological edge states in arrays of coupled nonlinear resonators in the pump-probe regime. When nonlinearity is weak, we observe that the frequencies of the resonators exhibit spectral shifts concentrated mainly at the edge mode and affecting only weakly the bulk modes. For a strong pumping, we describe several scenarios of the transformation of the edge states and their hybridization with bulk modes, and also predict a parametrically driven transition from topological stationary to unstable dynamic regimes.

Introduction. Topological photonics has recently emerged as a universal tool to achieve disorder-immune guiding of electromagnetic waves [1–5], but practical realizations of topological photonic devices require dynamic tunability. Despite the latest experiments on topological lasers [6–9] and several theoretical proposals for tunable nonlinear devices [10–16], experiments on reconfigurable topological structures are still scarce. Tuning of topological photonic edge states by temperature and liquid crystal orientation has been reported in [17] and [18], respectively. Another important recent milestone is the demonstration of nonlinearity-driven topological transition in electric circuits [19]. However, nonlinear tunability of topological electromagnetic edge states has not been shown so far and their fate in the nonlinear regime remains unclear.

In this Letter, we realize experimentally nonlinear spectral tuning of topological edge states of electromagnetic waves in one-dimensional arrays of identical electromagnetic resonators with Kerr-type nonlinearity. The resonators are separated by alternating long and short links, being coupled electromagnetically. Our concept is illustrated in Fig. 1. In the linear regime (a), an array of resonators is described by the Su-Schriffer-Heeger (SSH) model, and it represents a simple one-dimensional topological structure [20]. The system supports an electromagnetic topological mode localized at the edge terminated by the long link (the right edge in Fig. 1). This state occurs at the resonant frequency of an individual resonator being localized spectrally in the center of the band gap that appears due to a difference of the coupling coefficients for long and short links. When the structure is pumped homogeneously at the central frequency (see Fig. 1, left column), nonlinear spectral shifts of the resonator frequencies are induced. These spectral shifts modify the spectrum of linearized excitations, as shown in the bottom row of Fig. 1. Since the pump is at the resonance, the spectral shift is at its maximum for the edge resonator, affecting the corresponding edge state while the bulk spectrum remains mostly unchanged (Fig. 1f).

As such, even though the pump is homogeneous, the resonators are identical, and all tunneling coupling links are pump-independent (contrary to Refs. [19, 21]), the edge state exhibits a nonlinear spectral shift. At stronger pumping we expect that the edge state is destroyed due to its interaction with the bulk modes, while the nonlinear spectral shifts become large and identical for all the resonators.

While the nonlinear shift of the edge state frequency seems obvious, its inevitable destruction at high pumping is less evident. The nonlinear interaction between bulk and edge modes is still not understood and the physics of nonlinear topological systems is known to be very rich [11, 22–25]. In fact, at relatively low intensities the bulk modes are less affected by the nonlinearity than the edge state because the pump is in resonance with the linear edge state. At high pumping the edge state is non-
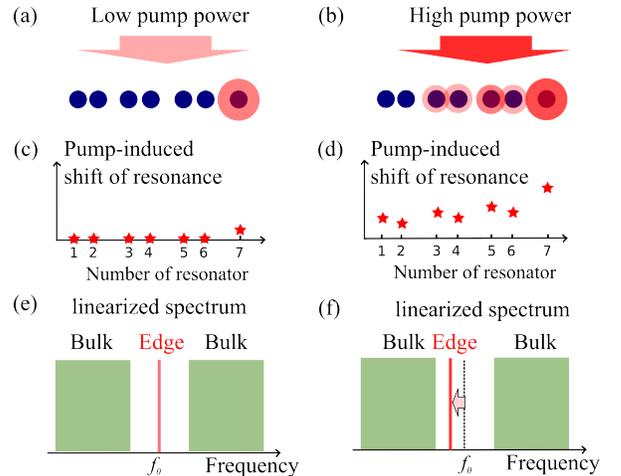
FIG. 1. (a,b) Arrays of resonators under (a,c,e) weak and (b,d,f) strong external homogeneous pumps. The pump is show by red colors. (c,d) Pump-induced spectral shifts of the resonant frequencies. (e,f) A change the linear spectrum of both bulk (green) and edge (red) states. A dashed vertical line marks the resonant frequency in the linear regime.

linearly detuned and its intensity becomes comparable with the bulk modes. So it is not obvious that the edge state must necessarily merge with the continuum. This fundamental question is inherent to the resonant nonlinear tuning, and differs our concept from nonresonant tuning mechanisms [17, 18]. Next, we present a rigorous theoretical model and then discuss experimental results in the pump-probe setup.

A topological chain of nonlinear oscillators. We consider a topological array of coupled oscillators with fast (instantaneous) cubic nonlinearity described by a system of equations

$$\frac{\mathrm{d}a_n}{\mathrm{d}t} = -\Gamma a_n - \mathrm{i}|a_n|^2 a_n + t_{n,-}a_{n-1} + t_{n,+}a_{n+1} + P \,, \quad (1)$$

where a_n is a normalized amplitude of the n-th oscillator ($n = 1 \ldots N$), Γ is a damping coefficient, and P is an amplitude of resonant homogeneous pump. Alternating strong and weak nearest-neighbor couplings are $t_{0,-} = t_{N,+} = 0$, $t_{2k,-} = t_{2k-1,+} = t_1$, $t_{2k,+} = t_{2k-1,-} = t_2$. The appropriate normalization allows one to set the coefficient in front of the nonlinear term to 1 without the loss of generality. Equation (1) can be applied to different systems [26, 27]. In the case of electromagnetic resonators, a_n stand for the slow-varying complex amplitudes of the current. Our goal is to find the stationary states excited by the pump and study the linear spectrum and stability.

We distinguish here two fundamentally different problems. In a general case, both nonlinear stationary states and linearized modes excited on the background of nonlinear solutions can be either localized or delocalized. When the pump is at the resonance, we expect a stationary localized nonlinear mode. On the other hand, the spectrum of linear excitations can include localized modes (such as edge states) as well. However, in those cases the corresponding pump dependencies differ for nonlinear stationary modes and linearized edge states.

First, we consider high-quality resonators ($\Gamma \ll |t_{1,2}|$). We study the chain of $N = 7$ resonators where a localized topological state is formed at the right edge ($n = N$) with weak link $|t_2| < |t_1|$. The results for stationary states are summarized in Fig. 2. Panel (a) shows the average amplitude in the bulk, defined as $|a_{1-6}|^2 = \sum_{n=1}^{6} |a_n|^2/6$, vs. the pump amplitude P. For $1 \lesssim P \lesssim 2$, these results suggest that our system exhibits bistability (red lines).

Our main goal is to study the edge states, so we examine a difference of the amplitude of the last oscillator and the amplitudes in the bulk oscillators. A localization strength can be defined by the edge-to-bulk ratio $\mu \equiv |a_7|/|a_{1-6}|$ shown in Fig. 3(b) as a function of the pump. At weak pump values, the localization parameter μ is considerable larger than unity indicating the presence of a stationary edge state. Indeed, from the spatial distribution of the stationary state [Fig. 3(c)] we observe that the amplitude is the largest for the last resonator.
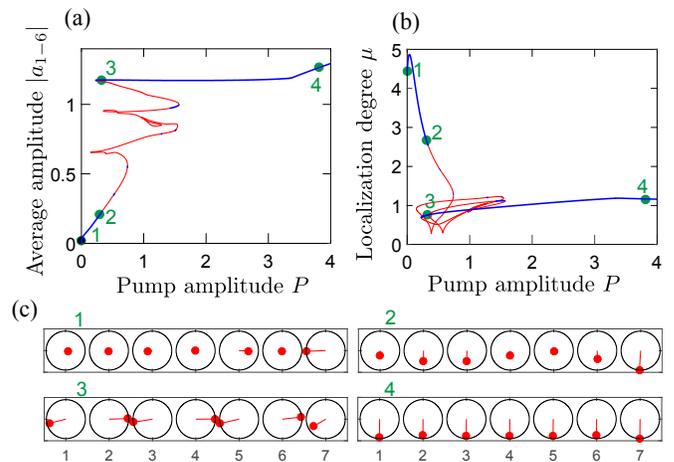
FIG. 2. (a) Average resonator amplitude $|a_{1-6}|$ and (b) localization degree μ for the amplitudes of the bulk and edge states vs. pump amplitude. Blue (red) lines correspond to linearly stable (unstable) solutions. Panel (c) shows spatial distributions of the normalized amplitudes at the points 1-4 on the bifurcation diagram. Distance of a red spot from the center of the ring is proportional to the absolute value of the amplitude, whereas the angle shows its phase with respect to the pump with in-phase oscillations corresponding to the direction to the left. Calculation parameters are $\Gamma = 0.02$, $t_1 = 1$, $t_2 = 0.48$.

The stationary edge state survives until the whole system looses its stability at a threshold pump value, as shown in Fig. 3(c) for the points 1 and 2 of the bifurcation diagram. For larger values of the pump, the edge state is eventually destroyed. Correspondingly, the localization parameter μ approaches unity, and the spatial distributions for the points 3 in Fig. 3(c) is more homogeneous.
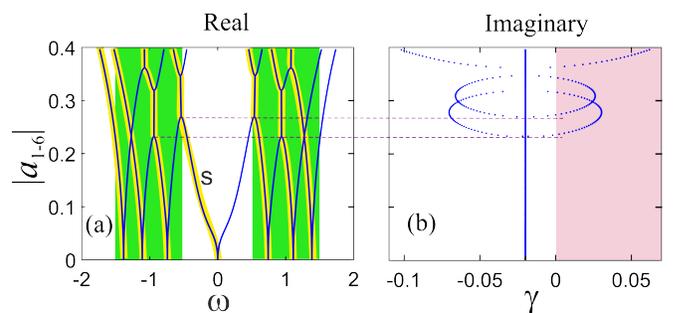
FIG. 3. Real (a) and imaginary (b) parts of the numerically calculated eigenfrequencies of the modes as functions of the average amplitude $|a_{1-6}| = \sqrt{\sum_{n=1}^{6} |a_n|^2/6}$. The eigenfrequencies with positive imaginary part [red area in panel (b)] correspond to the unstable modes. The yellow stripes show the approximate positions of the eigenvalues if the parametric effects are disregarded. The edge state is denoted as "s". The green rectangles show the frequencies of the continuum of the linear excitations on zero background. The calculation parameters are the same as in Fig. 2.

There exists a multistability regime where several different solutions can be supported by the same pump. Even if the edge state disappears the field distribution is not necessarily fully uniform. Due to the boundary effects the amplitudes of the edge resonators differ from those in the center of the structure, although no edge localization is evident, see (3) in Fig. 2(c). At even higher pumps the state becomes uniform, cf. (4) and (3) in Fig. 2(c).

Eigenvalues of the linear spectra on the background of nonlinear modes are shown in Fig. 3 as functions of the average intensity of six resonators. For weak intensities, the spectrum can be separated into the bulk modes lying inside the allowed bands of the infinite structure ($\omega \in \pm[t_1 - t_2 \ldots t_2 + t_2]$, green rectangles in Fig. 3(b)) and the edge mode ($\omega = 0$). Importantly, the linearization produces a parametric term $a_n^2 \delta a_n^*$, where δa_n is the excitation amplitude. Hence, the linear modes contain two parametrically coupled harmonics (cf. the Bogoliubov topological polaritonic modes in Ref. [28]). That is why the eigenfrequencies are double degenerate in the linear limit but at a finite pump the degeneracy is lifted. The yellow stripes mark the eigenvalues which are close to the eigenvalues of the system with omitted parametric term, and they have much larger excitation efficiency. In agreement with our expectations in Fig. 1, the central yellow stripe corresponding to the edge state (marked by "s") exhibits a nonlinear shift, much stronger than that for bulk modes.

If the pump becomes strong enough, the instability sets in, as seen from the imaginary parts of the eigenfrequencies in Fig. 3(b). At low intensities, the eigenfrequencies are purely real, then some of the eigenvalues collide producing pairs of complex conjugated eigenvalues. When the real part of an eigenvalue becomes positive (i.e., it enters the red region) the system acquires an exponentially growing perturbation and becomes unstable. Depending on parameters, the first instability can be produced by a collision of the edge state with a bulk mode or by a collision of two bulk modes. Summarizing the results in Figs. 2 and 3, we can claim that the mechanism of the edge state collapse is a dynamical instability developing in the system. The nonlinear stage of instability is studied by direct numerical simulations, and it is found that the system undergoes a complex dynamics.

However, the pump-dependent dependence described above is not the only scenario. In the case of higher losses, $\Gamma \gtrsim |t_{1,2}|$, the parametric instability becomes less important. The localization length of the edge state then grows monotonically with the pump due to hybridization with the bulk modes until it gets eventually delocalized while the system remains stable, see Fig. S1 and Fig. S2 in Supplementary Materials [29] for more details.

Pump-probe experiment. Our experimental results are presented in Figs. 4,5. In experiment, we have fabricated an array of $N = 7$ broadside-coupled split-ring resonators with the magnetic dipole resonance at the $f_0 \approx 1500$ MHz

frequency. The simplest way to tune the structure would be to modify its parameters mechanically [29, 30]. Here we focus on nonlinear tunability by varactor diodes that potentially allow dynamical tuning at the frequencies $\gtrsim 100$ MHz. A varactor diode has been mounted inside the gap of each ring to tune its frequency [29, 31]. The spectrum of linearized excitations, theoretically considered in Fig. 3, can be directly accessed in the spatially-resolved pump-probe setup. The experimental scheme is sketched in the inset of Fig. 4(d). The monochromatic homogeneous pump at the resonance $f = f_0$ has been provided by a rectangular horn antenna. The probe signal has been measured near each resonator by a small loop antenna connected to the receiving port of the analyzer. The probe spectrum of the reflection coefficient $\mathrm{Re}\,S_{11}$ for the loop antenna has been determined as a function of its position and the pump power.

Figures 4(a,b) show both theoretical and experimental spectra in the linear regime. A spectral signature of the edge state is clearly seen by the presence of the central resonance at the frequency f_0, when the probe is close to the right edge (black and magenta curves for $n = 5, 7$, respectively). Interestingly, the spectrum at the second-
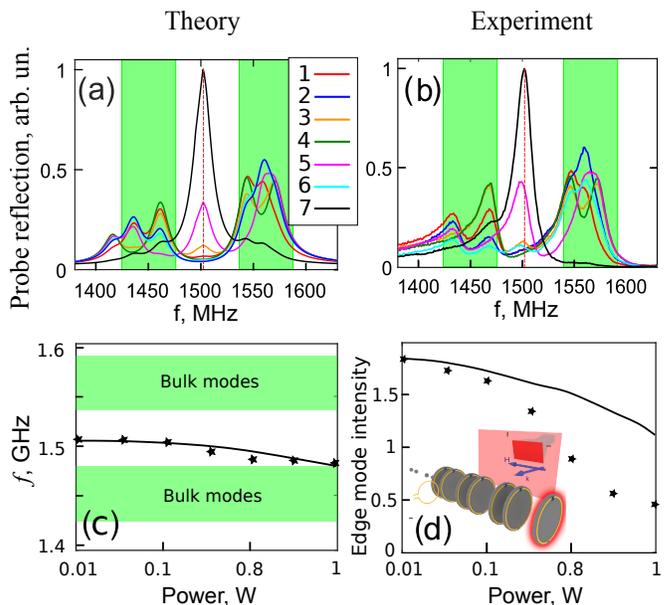
FIG. 4. (a,b) Spatially-resolved pump-probe spectra calculated numerically and measured experimentally. (c) Frequency of the edge state vs. pump power. A black solid line corresponds to theoretical results, and dots stand for experimental data. Green regions mark the allowed bands of an infinite structure calculated in the nearest-neighbor approximation. (d) A ratio of the amplitude of the spectral maximum associated with the edge state and the amplitude of the most intensive spectral maximum associated with a bulk mode. A blue solid line corresponds to numerical results and dots mark experimental data. Curves 1–7 correspond to the resonators from left to right.

to-last resonator, $n = 6$ (cyan curve) does not manifest a central resonance. This reflects the spatial structure of the edge state in the Su-Schrieffer-Heeger model, that, in the nearest-neighbor approximation, has nonzero amplitudes only at the modes with odd n. Other resonances in the spectrum correspond to bulk modes, and they are spectrally located within the allowed bands of the infinite array (shaded green rectangles). The coupling coefficients between the resonators are fitted to match the experimental spectrum with the initial values provided by the rigorous full-wave simulations in the CST Microwave Studio package. We also include the coupling of the resonators to the next neighbors which is taken to be ≈ 17 times weaker then the coupling in dimers, $t_3 = 0.06t_1$, with $t_1 = 55$ MHz, $t_2 = 0.48t_1$. The experimental pump power is related to the dimensionless amplitude in Eq. (1) as $P_{\mathrm{exp}}(\mathrm{W}) = 0.43 \cdot P^2$. More details are given in [29]. We take into account weak nonlocality of the probe, that senses the current not only in the nearest resonator but also in the adjacent resonators. Namely, the signal measured at n-th resonator is given by $E_n = a_n + \chi_1 a_{n+1} + \chi_2 a_{n-1} + \chi_3(a_{n+2} + a_{n-2})$ for odd n, and $E_n = a_n + \chi_1 a_{n-1} + \chi_2 a_{n+1} + \chi_3(a_{n+2} + a_{n-2})$, for even n, where the coupling coefficients are $\chi_1 = -0.12$, $\chi_2 = -0.1$ and $\chi_3 = -0.075$. A negative sign comes from anisotropy of the magnetic dipole. Nonlocality results in asymmetry of the excitation efficiencies for upper and lower allowed bands. Since the upper band corresponds to odd Bloch functions and $\chi_1 < 0$, it is sensed by a probe with higher efficiency than for the bottom band.

Our main experimental result is summarized in Fig. 4(c) for the edge state frequencies extracted from the probe spectra as a function of the pump power (raw spectra are given in Fig. S3 [29]). The central peak, corresponding to the edge mode, shifts with the pump power approaching the bulk bands. Experimental data (stars) are in a good agreement with our theory (black curve). This provides a direct experimental observation of the nonlinearly tunable electromagnetic topological edge state. We also compare the amplitude of the spectral maximum corresponding to the edge state to the most intense spectral maximum associated with a bulk mode. This ratio is plotted in Fig. 4(d) as a function of the pump power (stars). The edge state becomes less pronounced for higher pump intensities.

The destruction of edge state is reliably established but the specific mechanism is not obvious from experiment. The apparent absence of the discontinuities in the measured dependences on the pump power suggests that the instability does not take place. At low pump power, we observe a good agreement between the theory and experiment. The development of instability at high intensities is a more subtle issue depending on homogeneity, dispersion and nonlinearity of the resonators and diodes as well as on the accuracy of the fit parameters. Even the probe antenna itself introduces an inhomogeneity not ac-
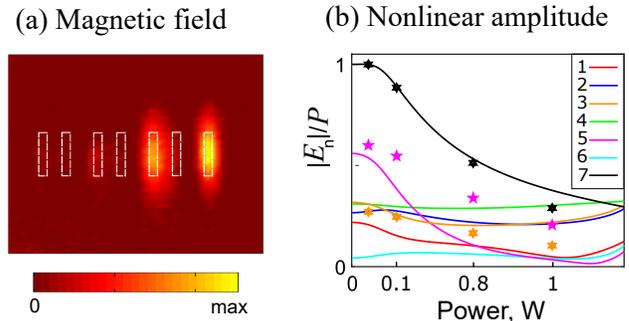
FIG. 5. (a) Magnetic field measured at the distance $l = 2$ mm from the structure. (b) A ratio of the normalized amplitudes of the bulk and edge resonators vs. pump power. Solid lines correspond to numerical simulations, and dots mark the experimental data.

counted by the model. The variation of the parameters of the diodes possibly explains why theoretical and experimental results match better in the linear regime. Moreover, the conservative cubic nonlinearity in Eq. (1) does not fully describe the real varactors. As a next approximation, we consider in [29] the role of dissipative nonlinearity and the decrease of the oscillator coupling to the pump at high pump strength. Account for such effects, presented in Figs. S4,S5 in [29] can significantly improve an agreement between theory and experiment. Further improvements would require consideration of saturable and non-instantaneous nonlinearity [32]. The quantitatively precise description is out of the scope of the present work. The main experimental result, nonlinear frequency tuning of edge state in Fig. 4(c) is well described by a simplistic model.

We also analyze a stationary map of the electromagnetic field at the pump frequency vs. pump power. Instead of measuring reflection S_{11} for an emitting probe loop antenna, we measure the transmission S_{12} from a horn antenna (a pump) to a probe. The input signal at the frequency f_0 is sent to the pump antenna only. Figure 5(a) shows the measured data for weak pump. The field localization directly visualizes the edge state. When the pump power increases, the stationary field becomes delocalized, as shown in Fig. 5(b) and Fig. S4 in [29]. Blue (black) stars show the power dependence for a ratio of the measured signal E to the pump power for the resonators with $n = 5$ and $n = 7$. In the same panel, we show the calculated dependencies of the same ratio E/P. The calculated amplitude for $n = 7$ matches experimental data reasonably well. The signal measured from the oscillator $n = 5$ has the second largest amplitude, and is well described by calculations. For large pump power, the stationary state becomes delocalized. A background of the signal, corresponding to $n < 5$, depends weakly on the pump power, being governed likely by long-range

couplings.

Conclusion. We have studied nonlinearity-induced tuning of the electromagnetic topological edge states in topological arrays of coupled nonlinear resonators with alternating weak and strong couplings. Combining nonlinear transmission and pump-probe experiments, we have demonstrated both stationary nonlinear states and linearized modes. We have revealed and described different scenarios of the pump-induced decay of topological states. Our results provide important insights into the physics of nonlinear tunable topological structures.

[1] L. Lu, J. D. Joannopoulos, and M. Soljačić, "Topological photonics," Nature Photonics **8**, 821–829 (2014).

[2] K. Y. Bliokh, F. J. Rodríguez-Fortuño, F. Nori, and A. V. Zayats, "Spin–orbit interactions of light," Nature Photonics **9**, 796–808 (2015).

[3] L. Lu, J. D. Joannopoulos, and M. Soljačić, "Topological states in photonic systems," Nature Physics **12**, 626–629 (2016).

[4] A. B. Khanikaev and G. Shvets, "Two-dimensional topological photonics," Nature Photonics **11**, 763–773 (2017).

[5] T. Ozawa, H. M. Price, A. Amo, N. Goldman, M. Hafezi, L. Lu, M. Rechtsman, D. Schuster, J. Simon, O. Zilberberg, and I. Carusotto, "Topological photonics," ArXiv e-prints (2018), arXiv:1802.04173 [physics.optics].

[6] P. St-Jean, V. Goblot, E. Galopin, A. Lemaître, T. Ozawa, L. L. Gratiet, I. Sagnes, J. Bloch, and A. Amo, "Lasing in topological edge states of a one-dimensional lattice," Nature Photonics **11**, 651 (2017).

[7] S. Barik, A. Karasahin, C. Flower, C. T, H. Miyake, W. DeGottardi, M. Hafezi, and E. Waks, "A topological quantum optics interface," Science **359**, 666 (2018).

[8] M. A. Bandres, S. Wittek, G. Harari, M. Parto, J. Ren, M. Segev, D. N. Christodoulides, and M. Khajavikhan, "Topological insulator laser: Experiments," Science **359**, eaar4005 (2018).

[9] C. E. Whittaker, E. Cancellieri, P. M. Walker, D. R. Gulevich, H. Schomerus, D. Vaitiekus, B. Royall, D. M. Whittaker, E. Clarke, I. V. Iorsh, I. A. Shelykh, M. S. Skolnick, and D. N. Krizhanovskii, "Exciton polaritons in a two-dimensional Lieb lattice with spin-orbit coupling," Phys. Rev. Lett. **120**, 097401 (2018).

[10] X. Zhou, Y. Wang, D. Leykam, and Y. D. Chong, "Optical isolation with nonlinear topological photonics," New J. Phys. **19**, 095002 (2017).

[11] Y. V. Kartashov and D. V. Skryabin, "Bistable topological insulator with exciton-polaritons," Phys. Rev. Lett. **119**, 253904 (2017).

[12] E. Saei Ghareh Naz, I. Cosma Fulga, L. Ma, O. G. Schmidt, and J. van den Brink, "Topological phase transition in a stretchable photonic crystal," ArXiv e-prints (2017), arXiv:1712.01678 [cond-mat.mes-hall].

[13] Z. Song, H. Liu, N. Huang, and Z. Wang, "Electrically tunable robust edge states in graphene-based topological photonic crystal slabs," J. Phys. D **51**, 095108 (2018).

[14] R. K. Pal, J. Vila, M. Leamy, and M. Ruzzene, "Amplitude-dependent topological edge states in nonlinear phononic lattices," Phys. Rev. E **97**, 032209 (2018).

[15] D. D. Solnyshkov, O. Bleu, and G. Malpuech, "Topological optical isolator based on polariton graphene," Appl. Phys. Lett. **112**, 031106 (2018).

[16] R. S. Savelev, M. A. Gorlach, and A. N. Poddubny, "Topological interface states mediated by spontaneous symmetry breaking," Phys. Rev. B **98**, 045415 (2018).

[17] L. Chong, H. Xiaoyong, G. Wei, A. Yutian, C. Saisai, Y. Hong, and G. Qihuang, "Thermo-optical tunable ultracompact chip-integrated 1d photonic topological insulator," Advanced Optical Materials **6**, 1701071.

[18] M. I. Shalaev, S. Desnavi, W. Walasik, and N. M. Litchinitser, "Reconfigurable topological photonic crystal," New J. Phys. **20**, 023040 (2018).

[19] Y. Hadad, J. C. Soric, A. B. Khanikaev, and A. Alù, "Self-induced topological protection in nonlinear circuit arrays," Nature Electronics **1**, 178–182 (2018).

[20] S.-Q. Shen, *Topological Insulators. Dirac Equation in Condensed Matters*, Springer Series in Solid-State Sciences (Springer, Heidelberg, 2013).

[21] Y. Hadad, A. B. Khanikaev, and A. Alù, "Self-induced topological transitions and edge states supported by nonlinear staggered potentials," Phys. Rev. B **93**, 155112 (2016).

[22] D. Leykam and Y. D. Chong, "Edge solitons in nonlinear-photonic topological insulators," Phys. Rev. Lett. **117**, 143901 (2016).

[23] D. D. Solnyshkov, A. V. Nalitov, and G. Malpuech, "Kibble-Zurek mechanism in topologically nontrivial zigzag chains of polariton micropillars," Phys. Rev. Lett. **116**, 046402 (2016).

[24] Y.-R. Zhang, Y. Zeng, H. Fan, J. Q. You, and F. Nori, "Characterization of topological states via dual multipartite entanglement," ArXiv e-prints (2017), arXiv:1712.05286 [quant-ph].

[25] A. N. Poddubny and D. A. Smirnova, "Ring Dirac solitons in nonlinear topological systems," Phys. Rev. A **98**, 013827 (2018).

[26] B. G.-g. Chen, N. Upadhyaya, and V. Vitelli, "Nonlinear conduction via solitons in a topological mechanical insulator," Proc. Nat. Acad. Sci. **111**, 13004–13009 (2014).

[27] D. D. Solnyshkov, O. Bleu, B. Teklu, and G. Malpuech, "Chirality of topological gap solitons in bosonic dimer chains," Phys. Rev. Lett. **118**, 023901 (2017).

[28] C.-E. Bardyn, T. Karzig, G. Refael, and T. C. H. Liew, "Chiral Bogoliubov excitations in nonlinear bosonic systems," Phys. Rev. B **93**, 020502 (2016).

[29] See online Supplementary Materials.

[30] X. Cheng, C. Jouvaud, X. Ni, S. H. Mousavi, A. Z. Genack, and A. B. Khanikaev, "Robust reconfigurable electromagnetic pathways within a photonic topological insulator," Nature Materials **15**, 542 (2016).

[31] D. Filonov, Y. Kramer, V. Kozlov, B. Malomed, and P. Ginzburg, "Resonant meta-atoms with nonlinearities on demand," Appl. Phys. Lett. **109**, 111904 (2016).

[32] M. A. Gorlach, D. A. Dobrykh, A. P. Slobozhanyuk, P. A.

Belov, and M. Lapine, "Nonlinear symmetry breaking in photometamaterials," Phys. Rev. B **97**, 115119 (2018).